Journal of Alloys and Compounds 509 (2011) 4929–4934

Contents lists available at ScienceDirect

Journal of Alloys and Compounds

journal homepage: www.elsevier.com/locate/jallcom

First-principles study of the ferroelectric and optical properties of $BaTeMo_2O_9$

J. Zhang[a,*], X.F. Li[a], B. Xu[a], K.L. Yao[b]

[a] School of Mathematics and Information Science, North China University of Water Resources and Electric Power, Zhengzhou 450011, China
[b] School of Physics, Huazhong University of Science and Technology, Wuhan 430074, China

ARTICLE INFO

Article history:
Received 18 October 2010
Received in revised form 19 January 2011
Accepted 30 January 2011
Available online 24 February 2011

PACS:
42.70.Mp
31.15.Ar
77.22−d

Keywords:
First-principles
Spontaneous polarization
Berry phase method
Nonlinear optical property

ABSTRACT

Electronic structure, spontaneous polarization and optical properties of single crystal $BaTeMo_2O_9$ have been investigated based on density-functional theory. It is found that $BaTeMo_2O_9$ has a direct-band-gap of 2.78 eV and there exists obvious hybridization between O 2p–Te 5p and O 2p–Mo 4d states. The results show that this compound is a good ferroelectric with large spontaneous polarization, which mainly arises from the strong Te–O and Mo–O hybridization. The interband contributions to the peaks of the optical spectra are discussed in details. Furthermore, the nonlinear optical properties are calculated by using $2n+1$ theorem applied to an electric-field dependent energy functional. The large NLO susceptibilities reveal that $BaTeMo_2O_9$ is a high-performance NLO crystal.

1. Introduction

In recent years, noncentrosymmetric (NCS) compounds have attracted great interest in materials chemistry because of their important symmetry-dependent properties, such as ferroelectricity, piezoelectricity, and second-order nonlinear optical (NLO) behaviors [1–6]. In searching for NCS compounds, much attention has been paid to oxides including the second-order Jahn–Teller (SOJT) distortion cations [7,8] such as d^0 transition metal ions (Ti^{4+}, Mo^{6+}, etc.) and cations with stereochemical activity of a lone pair electrons of ns^2 (Pb^{4+}, Bi^{3+}, etc.). Both kinds of ions are susceptible to SOJT distortion for a nondegenerate ground state interacting with the low-lying exciting state [9].

In this paper, we mainly pay our attention to a noteworthy NCS oxide $BaTeMo_2O_9$. In 2003, polycrystalline $BaTeMo_2O_9$ was synthesized by the solid-state reaction method by Ra et al. [9]. They observed the extremely strong power second-harmonic generation (SHG) efficiencies (about $600 \times SiO_2$) which attributes from the polarization attributing to the Te^{4+}–O and Mo^{6+}–O bonds constructively add [9]. In 2007, single crystal $BaTeMo_2O_9$ (space group $P2_1$, $a = 5.5346$ Å, $b = 7.4562$, $c = 8.8342$ Å, $\beta = 90.897^\circ$, $Z = 2$) was synthesized from a TeO_2–MoO_3 system by the flux method by Tao et al. [10]. As a multifunctional NCS compound, the refractive index, electro-optic tensor, dielectric and piezoelectric properties of single crystal $BaTeMo_2O_9$ were also measured by them [10–12]. Their experimental data revealed that $BaTeMo_2O_9$ is not only a potential nonlinear optical crystal but also a promising piezoelectric material. In Fig. 1, we present the crystallographic structure of single crystal $BaTeMo_2O_9$.

Nowadays, first-principles calculations based on density functional theory (DFT) to predict the accurate properties of the new materials can meet the requirements of the experimentalists for a helpful theoretical data. We know that the optical measurements on crystals require not only the superexcellent quality compounds but also a special laboratory, at the same time, it is usually expensive. Therefore, first-principles as an alternative for predicting the optical properties can help us to interpret the experimental results by investigating the microscopic structure of the compounds. Based on the group theory, the space group $P2_1$ of $BaTeMo_2O_9$ belong to the point group 2 (C_2^2), which is the spontaneous polarization point group. Therefore, single crystal $BaTeMo_2O_9$ should be a promising ferroelectric material. However, until now, as far as we know there are no reports about the spontaneous polarization of $BaTeMo_2O_9$. Using first-principles calculations based on density functional theory, we have investigated the electronic structure, spontaneous polarization and optical properties of single crystal $BaTeMo_2O_9$. In addition, as materials with the point group C_2^2 usually exhibit nonlinear optical properties, we also calculate its nonlinear susceptibilities by using $2n+1$ theorem [13,14] applied to an electric-field dependent energy functional.

* Corresponding author.
E-mail address: zhangjing@ncwu.edu.cn (J. Zhang).

0925-8388/$ – see front matter © 2011 Elsevier B.V. All rights reserved.
doi:10.1016/j.jallcom.2011.01.171

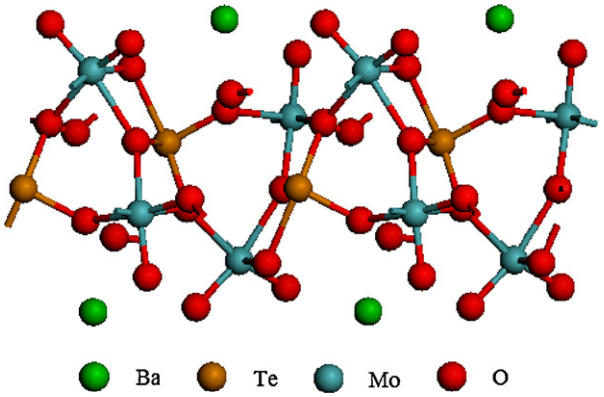

Fig. 1. A view of the crystal structure of single crystal $BaTeMo_2O_9$ along the *y*-axis.

2. Computational method

In this work, we adopt the ABINIT package [15], a plane-wave pseudopotential (PWPP) DFT code, which allows not only the usual ground-state calculations but also the linear-response computations of phonons frequency, Born effective charges, spontaneous electric polarization, dielectric, and piezoelectric tensors [16,17]. The geometry optimization, electronic structure, and optical properties are calculated by adopting the ultrasoft pseudopotentials, which are generated by the scheme of Vanderbilt [18]. We use a plane wave cut off of 40 hartrees, with an $8 \times 8 \times 8$ Monkhorst–Pack *k*-point mesh [19], and the Perdew–Burke–Ernzerhof functional (PBE) [20] of GGA as exchange correlation potential. The Ba 6s electrons, Te 5s and 5p electrons, Mo 4d and 5s electrons, as well as O 2s and 2p electrons are considered as valence states in the construction of the pseudopotentials. In order to obtain nonlinear optical properties, we use norm-conserving pseudopotentials according to the Troullier–Martins scheme [21] with local density approximation (LDA) as the exchange correlation potential. We adopt a plane wave cut off of 45 hartrees, with a mesh of $8 \times 8 \times 8$ Monkhorst–Pack *k*-point.

For the linear and nonlinear response computations, the technical details on the computation of responses to atomic displacements, homogeneous electric fields, and strains are based on the density-functional perturbation theory (DFPT) [22,23]. In order to obtain the nonlinear optical susceptibilities, we present the computation of third-order energy derivatives based on $2n+1$ theorem, computation of energy derivatives up to third order only requires the knowledge of the ground-state and first-order wave functions. Considering the three Hermitian perturbations (λ_1, λ_2, and λ_3), the mixed third-order derivatives can be calculated from the ground state wave functions,

$$E^{\lambda_1\lambda_2\lambda_3} = \frac{1}{6}\frac{\partial^3 E}{\partial\lambda_1\lambda_2\lambda_3}\bigg|_{\lambda_1=0,\lambda_2=0,\lambda_3=0} \quad (1)$$

In an insulator, the electric polarization can be expressed as a Taylor expansion of the macroscopic electric field,

$$P_i = P_i^s + \sum_{j=1}^{3} x_{ij}^{(1)}\varepsilon_j + \sum_{j,l=1}^{3} x_{ijl}^{(2)}\varepsilon_j\varepsilon_l + \cdots, \quad (2)$$

where P_i^s, $x_{ij}^{(1)}$, and $x_{ijl}^{(2)}$ are the zero-field spontaneous polarization, linear dielectric constant, and second-order nonlinear optical susceptibility [24], respectively. For the nonlinear optical susceptibility, we only consider the electronic contribution (with the ions at clamped positions) and the third-order derivative of the energy with respect to low-frequency electric fields,

$$\chi_{ijl}^{(2)} = -\frac{3}{\Omega_0}E^{\varepsilon_i\varepsilon_j\varepsilon_l} \quad (3)$$

Based on above definition in Eq. (2), we can obtain the nonlinear optical susceptibility when considering these electric fields as the three perturbations. In addition, it is well-suited to adopt another definition of the nonlinear optical susceptibility *d* tensor instead of $x_{ijl}^{(2)}$ ($d_{ijl} = (1/2)x_{ijl}^{(2)}$).

Table 1
The theoretical and experimental lattice constants and volume of single crystal $BaTeMo_2O_9$.

$BaTeMo_2O_9$	*a* (Å)	*b* (Å)	*c* (Å)	*V* (Å^3)
Expt Ref. [9]	5.5346	7.4562	8.8342	374.35
Cal (GGA)	5.6849	7.5721	8.9373	384.71

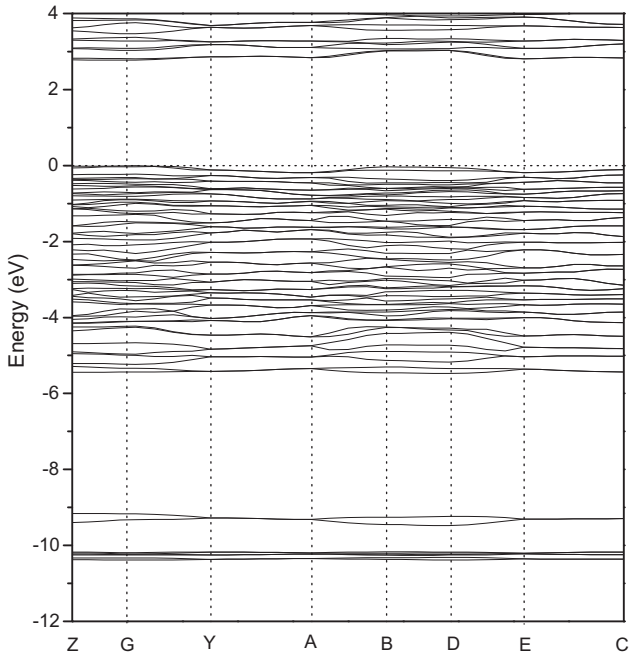

Fig. 2. Band structure of single crystal $BaTeMo_2O_9$ along the high symmetry directions in the Brillouin zone.

3. Results and discussion

3.1. Electronic structure

In order to obtain the optimal geometry of single crystal $BaTeMo_2O_9$, we carry out both geometric optimization and atomic relaxation from the experimental lattice parameters to find the equilibrium configuration until the change of the total energy in the self-consistent calculations are less than 10^{-7} eV, and the remaining forces on the atoms are less than 10^{-5} hartree/bohr. In Table 1, we present the experimental and theoretical lattice parameters of this compound. The calculated lattice parameters are in good agreement with the experimental data.

Then, we perform the electronic structure calculations of $BaTeMo_2O_9$ according to the optimized lattice parameters. In Fig. 2, we present the energy band structure along the high-symmetry lines in the first Brillouin zone in the energy range of −12–4 eV. From Fig. 2, it is found that the top of the valence band (VB) and the bottom of the conduction band (CB) are both at the *G* (0.0, 0.0, and 0.0) point and the direct band gap (E_g) is about 2.78 eV. Generally, the band gaps predicted by DFT are smaller than experimental

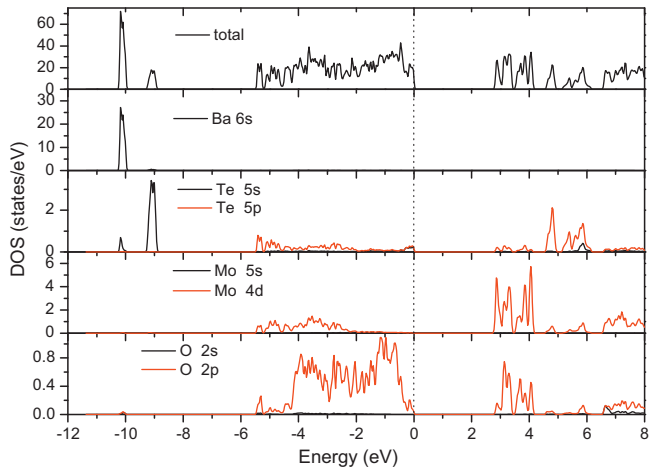

Fig. 3. Total and partial density of states of $BaTeMo_2O_9$. The Fermi level is set at 0 eV.

data, so the E_g of this compound should be larger. In order to further investigate the electronic structure of single crystal $BaTeMo_2O_9$, we divide the occupied band structure into the three energy regions: (i) bands lying from −11 to −9 eV, (ii) bands lying from −6 to −2 eV, and (iii) bands within the range from −2 to 0 eV.

In Fig. 3, we give the total and partial density of states (DOSs) of this compound. By investigating the energy band structure and DOSs, it is found that region (i) contains 8 bands, which come from Ba 6s, Te 5s, O 2s and 2p orbitals. For the total DOS, two sharp peaks at 10.25 and 9.3 eV are clearly visible; regions (ii) includes 30 bands, which mostly arise from Te 5p, Mo 4d, and O 2p electrons, among them it is found that the DOSs between O 2p and Te 5p, Mo 4d electrons have similar peaks and character, which reveal that there exists strong hybridization between O 2p–Te 5p and O 2p–Mo 4d states; region (iii) with 24 bands mainly come from O 2p, Te 5s and 5p electrons, and with small contribution from Mo 4d electrons. Above the Fermi level (E_f), the conduction band is dominated by Mo 4d, O2p, and Te 5s states.

3.2. Spontaneous polarization

As the space group of single crystal $BaTeMo_2O_9$ is $P2_1$, which belongs to the polar point group 2 (C_2^2), one of the 10 polar point groups (C_1, C_2, C_3, C_4, C_6, C_m, C_{2v}, C_{3v}, C_{4v}, C_{6v}) required for ferroelectric characteristic. The modern theory of polarization [25–29] provides the correct definition of P_s, as well as the theoretical framework allowing one to compute it from the occupied Bloch eigenvectors of the self-consistent crystalline Hamiltonian. In addition, we know that the atomic charge definitions can be categorized in either static, based on the partitioning of the charge density into contributions to the specific atoms, or Born effective charges (Z^*), defined by the change in polarization created by atomic displacement. The Born effective charges tensors can be expressed as

$$Z^*_{i,\alpha,\beta} = \frac{\Omega}{e}\frac{\partial P_\beta}{\partial u_{i,\alpha}} = \frac{\Omega}{e}\frac{\partial F_{i,\alpha}}{\partial E_\beta} \quad (4)$$

where Z^* is the polarization per unit cell induced by displacement of atomic i in direction α or the force exerted on atom by macroscopic electric field in the direction β. The Born effective charges (Z^*) plays a fundamental role in understanding the polar ground state and lattice dynamics. In this section, we mainly investigate Z^* and spontaneous polarization of single crystal $BaTeMo_2O_9$.

By calculating the linear response to atomic displacements (phonon) and homogeneous electric fields, we get the Born effective charge tensors of $BaTeMo_2O_9$ based on Eq. (4). The obtained

Table 2
Born effective charges (in atomic units) of Ba, Te, Mo_{1-2}, O_{1-9} in the single crystal $BaTeMo_2O_9$.

Atom	Z^*_{xx}	Z^*_{yy}	Z^*_{zz}	Z^*_{xy}	Z^*_{xz}	Z^*_{yz}	Z^*_{yx}	Z^*_{zx}	Z^*_{zy}
Ba	2.65	2.96	3.92	0		0.13	0.23	0.20	−0.05 0.24
Te	2.67	4.29	3.77	0.47		−0.16	0.12	0.93	0.64 0.49
Mo_1	6.79	6.59	4.10	1.37		1.12	0.26	0.41	−0.03 −0.34
Mo_2	5.85	6.60	4.54	0.84		−0.20	0.18	1.47	0.54 0.06
O_1	−1.84	1.78	2.56	0.82		0.32	0.46	0.27	0.12 0.82
O_2	−1.36	3.52	1.42	0.34		−0.25	0.52	1.17	0.06 0.59
O_3	−2.37	2.11	2.02	0.76		0.26	0.60	1.09	−0.36 0.62
O_4	−2.85	2.06	2.02	1.62		−0.29	0.27	1.10	−0.10 0.47
O_5	−2.20	2.14	1.27	0.85		−0.74	0.85	0.99	−0.31 0.56
O_6	−0.93	2.39	2.12	0.11		−0.01	1.39	0.15	−0.02 1.07
O_7	−3.52	3.43	0.98	2.17		0.30	0.23	2.66	0.25 0.23
O_8	−1.83	1.99	0.67	0.99		0.17	0.01	0.89	0.09 0.02
O_9	−1.05	0.99	3.26	0.13		−0.66	0.35	0.14	−0.84 0.29

Z^* from the two different perturbations are same, we give these results in Table 2. As Z^* can reflect the covalence of the bonding environment of each atom with respect to their nominal ionic value, and the nominal ionic value of Ba, Te, Mo, O are +2, +4, +6, and −2. By comparing the ionic values with Born effective charges, it is found that Z^* of O_2 and O_7 (yy component) are obviously far more anomalous than those of the rest atoms. According to the crystal structure of this compound in Fig. 1, due to Mo_1 and Mo_2 are located in the similar octahedron of O atoms, Z^* of Mo_1 and O_7 (yy component) are nearly equal, which reveal that Mo_1 and Mo_2 make the same contribution to the spontaneous polarization (along y-axis).

In order to calculate the spontaneous polarization, we adopt the Berry phase method developed by Resta [25], King-Smith and Vanderbilt [28,29]. In this work, we have calculated the spontaneous polarizations of single crystal $BaTeMo_2O_9$ by a finite electric field method based on the Berry phase model. In the finite electric field calculations, first, along the different crystal directions, we adopt a series of positive weak homogeneous electric fields as perturbation to obtain a series of electric polarizations until these values tend to saturation. Next, similarly, using a series of weak negative homogeneous electric fields as perturbation, we get almost the same absolute value of the saturated electric polarization. The total polarization P for a certain material is the sum of the ionic polarization P_{ion} and electronic polarization P_{ele}. Along the x, y, and z axes, the obtained spontaneous polarization P_x, P_y, and P_z of this compound are 0, 11.87 and 0 μC/cm^2, respectively. As the values of P_x and P_z are zero, the spontaneous polarization is mainly along the y-axis. Moreover, the calculated results reveal that the ionic and electronic polarization P_{ion} and P_{ele} are −7.28 and 19.15 μC/m^2, respectively.

4. Linear and nonlinear optical properties

Generally, in condensed matter systems there are two contributions to the complex dielectric function, viz. intraband and interband transitions. In our dielectric function calculation we only consider the electronic excitations and neglect the phonons effect. The imaginary part of the dielectric function is given by

$$\varepsilon_2(\omega) = \left(\frac{Ve^2}{2\pi\hbar m^2\omega^2}\right)\sum_{i,j}\int_{BZ} d^3k \sum_{nn'} \left|\langle kn|\, p\, |kn'\rangle\right|^2 f_{kn} \times (1 - f_{kn'})\delta(E_i - E_j - \hbar\omega) \quad (5)$$

where $\hbar\omega$ is the energy of the incident phonon, p is the momentum operator, $|kn\rangle$ is a crystal wave function, f_{kn} the Fermi–Dirac distribution function, e and m represent the charge and the mass of electron, the subscripts i and j denote the conduction and the valence bands, respectively. We know that the imaginary part of

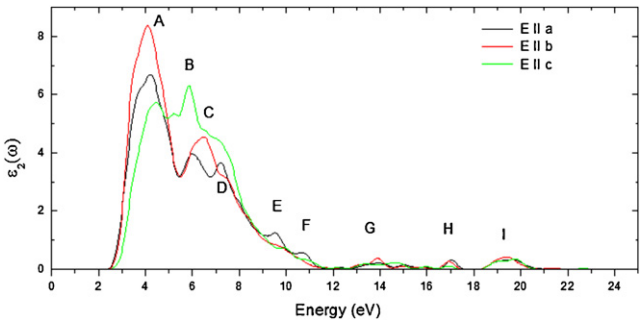

Fig. 4. Imaginary part of the dielectric function of $BaTeMo_2O_9$ corresponding to the electric field parallel to *a*, *b*, and *c* direction, respectively.

the dielectric function is the pandect of the optical properties for any materials. With the help of the Kramers–Kronig transformation [30,31], the real part $\varepsilon_1(\omega)$ can be calculated from the imaginary part $\varepsilon_2(\omega)$. In addition, the other optical constants (refractive index, reflectivity, and absorption coefficient et al.) can derive from the complex dielectric function. To avoid the theoretical error caused from the underestimate the band gap in DFT, the scissor approximation [32–34] is widely used. In this work, we do not consider the scissor approximation due to the lack of experimental band gap of $BaTeMo_2O_9$.

In Fig. 4, we give the frequency dependence dielectric functions $\varepsilon_2^a(\omega)$, $\varepsilon_2^b(\omega)$ and $\varepsilon_2^c(\omega)$ corresponding to the electric field parallel to *a*, *b* and *c*-axis, respectively. It is found that the dielectric tensors show obvious anisotropy. The spectra corresponding to $E||a$, $E||b$, and $E||c$ are different below 11 eV; however there is less difference among them above 11 eV, which reveals the spectral anisotropy occurs mainly within the lower energy region. In order to investigate the three different frequency dependence dielectric functions, we divide their peaks into four parts within the energy range: (i) 0–5 eV (A), (ii) 5–12 eV (B, C, D, E, and F), and (iii) 12–20 eV (G, H, and I). The lowest-energy peaks in range (i) are at around 4 eV, which is dominated by the transition from top of the valences bands to the conductions bands. These peaks mainly result from interband transitions (O 2p to Mo 4d and Te 5p orbitals). The peaks in region (ii) mainly arise from O 2p to Mo 4d and Te 5p. In the high energy region (iii), the small peaks are due to transitions from lower-lying occupied level to higher-lying unoccupied levels. These peaks mainly originate from the transitions from O 2s, 2p valences bands to Mo 4d and Te 5p high-energy conduction bands.For a crystal, the refractive indices can relate to the electronic polarizability of ions and the local field inside the crystal. Moreover, they are also connected to the electro-optical effect, and in ferroelectrics the spontaneous polarization can induce the spontaneous electro-optical effect in the ferroelectric phase. In Fig. 5, we present the real part $n(\omega)$ of refractive index. In order to compare our results with experimental values [9], we give the refractive indices $n(\lambda)$ as a function of wave λ. It is noted that the polarization directions of the two orthorhombic refractive indices n_x and n_y are in the ac-plane, and n_z is parallel to crystallographic *b*-axis. From Fig. 5, it is found that in the range of the short wavelength between 0.4 and 0.6 μm, the refractive indices are slightly larger than the experimental values; in the range of wavelength between 0.6 and 1.1 μm, the results are in good agreement with the experimental values.

The reflectivity $R(\omega)$, absorption coefficient $I(\omega)$, extinction coefficient $k(\omega)$, and energy-loss spectrum $L(\omega)$ are presented in Fig. 6. Generally, the peaks of the energy-loss spectrum $L(\omega)$ show the characteristic associated with the plasma response and the corresponding frequency is the so-called plasma frequency, above which the material exhibits the dielectric behavior [$\varepsilon_1(\omega) > 0$], however below which the material displays the metallic properties [$\varepsilon_1(\omega) < 0$]. Because of the peaks in $L(\omega)$ spectra are the points corresponding to transition from metallic character to dielectric property, we find that in the vicinity of locations of 12, 14, 20 and 39 eV the one prominent peaks located and other three small peaks are consistent with $\varepsilon_1(\omega)$. Furthermore, the peaks of energy-loss spectra corresponding to the abrupt reduction of $L(\omega)$ can be seen Fig. 6. Except refractive index, there are no other optical constants can make reference to the experimental values, so our study can be as a prediction of the optical properties.

As a NLO material, as mentioned by Ra et al. [9], the large SHG response of $BaTeMo_2O_9$ mainly arise from the polarizations due to the Mo^{6+}–O and Te^{4+}–O bonds constructively add. However, until now, as far as we know there are no reports about the NLO susceptibilities of $BaTeMo_2O_9$. Using $2n+1$ theorem applied to an electric-field dependent energy functional, we perform the theoretical calculations of the NLO susceptibilities of this compound. According to the calculated results, we find that the NLO

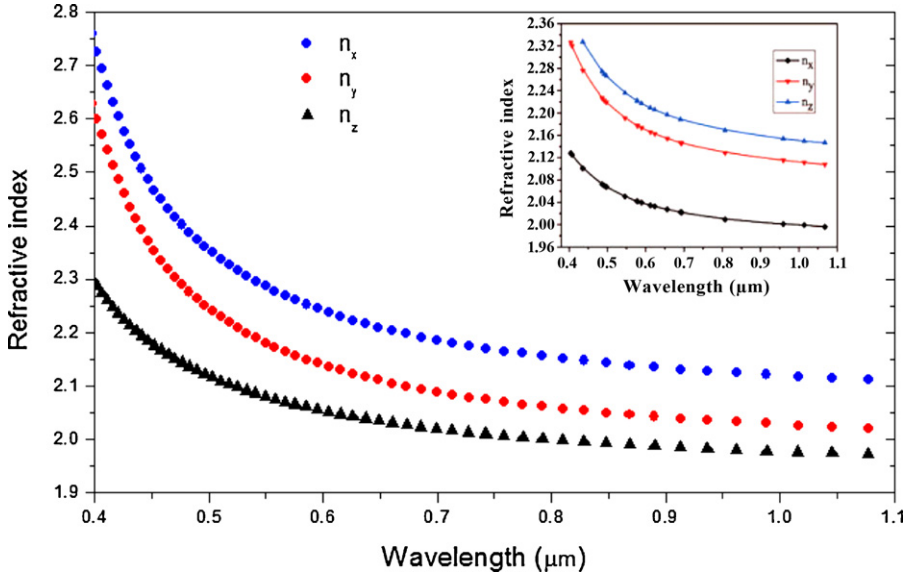

Fig. 5. The calculated and experimental (illustration) frequency-dependent refractive indices $n(\lambda)$ of single crystal $BaTeMo_2O_9$.

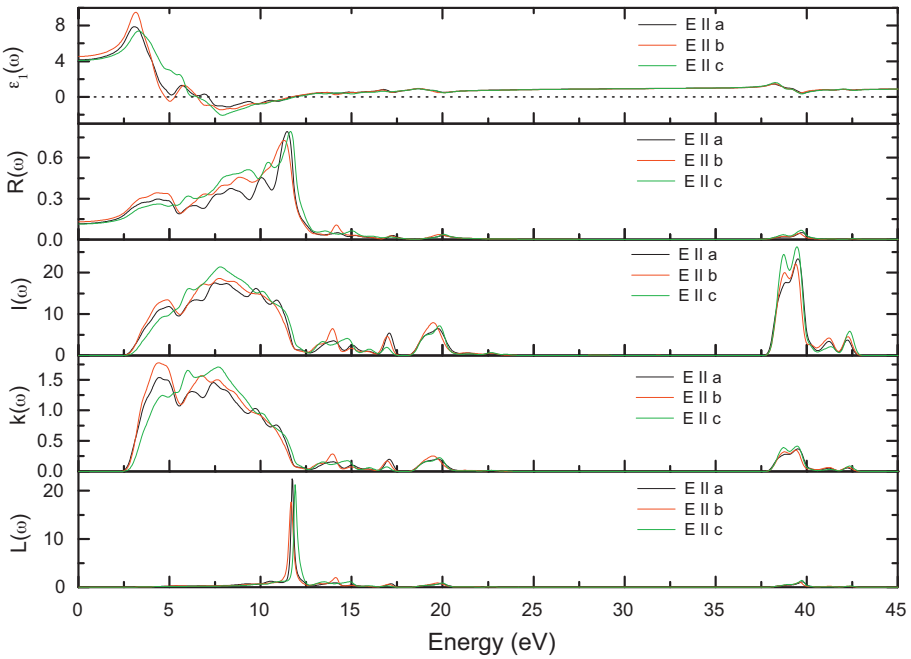

Fig. 6. The calculated frequency-dependent optical constants: real part of the dielectric function $\varepsilon_1(\omega)$, reflectivity $R(\omega)$, absorption coefficient $I(\omega)$, extinction coefficient $k(\omega)$, and energy-loss spectrum $L(\omega)$.

susceptibilities of single crystal $BaTeMo_2O_9$ have four independent elements (Voigt notations) d_{14}, d_{21}, d_{22}, d_{23}:

$$d = \begin{pmatrix} 0 & 0 & 0 & d_{14} & 0 & d_{21} \\ d_{21} & d_{22} & d_{23} & 0 & d_{14} & 0 \\ 0 & 0 & 0 & d_{23} & 0 & d_{14} \end{pmatrix} \quad (6)$$

The values of the four independent elements d_{14}, d_{21}, d_{22}, d_{23} are 2.22, −1.41, −3.38, and −3.15 pm/V, respectively. The large nonlinear susceptibilities reveal that $BaTeMo_2O_9$ is a promising NLO material.

5. Conclusion

In this paper, we have investigated the electronic structure, Born effective charges, spontaneous polarization, linear and nonlinear optical properties of single crystal $BaTeMo_2O_9$ in the framework of density functional theory.

The electronic structure shows that $BaTeMo_2O_9$ is an insulator with a direct-band-gap of 2.78 eV and the O 2p states are strong hybridized with Te 5p and Mo 4d states. The spontaneous polarization and Born effective charges (Z^*) are calculated based on a Berry-phase approach. It is found that single crystal $BaTeMo_2O_9$ is a good ferroelectric with the large spontaneous polarization (P_s = 11.87 μC/cm^2). The polarized direction is along the *y*-axis. By investigating the Born effective charge of this compound, we find that Z^* of O and Mo atoms show relatively large anomalous behavior. The strong Te–O and Mo–O hybridization is the mainly source for the large spontaneous polarization.

With the help of the Kramers–Kronig transformation, we calculate the complex dielectric function and the corresponding optical properties. For the imaginary part of dielectric function, we analyze the interband contributions to the different peaks. The optical spectra are assigned to interband contribution between O 2p valence bands to Mo 4d conduction bands in the low-energy region and between O 2p valence bands and Te 5s, 5p conduction bands in the high-energy region. The calculated refractive index is in good agreement with the experimental values. Using $2n+1$ theorem applied to an electric-field dependent energy functional, we perform the theoretical calculations of the NLO susceptibilities of single crystal $BaTeMo_2O_9$. We find that single $BaTeMo_2O_9$ has four independent elements (Voigt notations) d_{14}, d_{21}, d_{22}, and d_{23}, and their values are 2.22, −1.41, −3.38, and −3.15 pm/V, respectively. The large nonlinear susceptibilities reveal that $BaTeMo_2O_9$ is a promising NLO crystal.

Acknowledgments

This work was supported by China 973 plan (No. 2006CB921605), the National Natural Science Foundations of China (Nos. 10804034, 10947162 and 10774051) and the Research Fund for the Doctoral Program of Higher Education of China (No. 20090142110063).

References

[1] P.S. Halasyamani, K.R. Poeppelmeier, Chem. Mater. 10 (1998) 2753.
[2] O. Auciello, J.F. Scott, R. Ramesh, Phys. Today 51 (1998) 22.
[3] S.B. Lang, Phys. Today 58 (2005) 31.
[4] A. Frau, J.H. Kim, P.S. Halasyamani, Solid State Sci. 10 (2008) 1263–21268.
[5] H.Y. Chang, S.H. Kim, P.S. Halasyamani, K.M. Ok, J. Am. Chem. Soc. 131 (2009) 2426–2427.
[6] J. Zhang, K.L. Yao, Z.L. Liu, G.Y. Gao, S.Y. Sun, S.W. Fan, Phys. Chem. Chem. Phys. 12 (2010) 9197.
[7] R.G. Pearson, J. Am. Chem. Soc. 91 (1969) 4947–4955.
[8] R.A. Wheeler, M.-H. Whangbo, T. Hughbanks, R. Hoffmann, J.K. Burdett, T.A. Albright, J. Am. Chem. Soc. 108 (1986) 2222–2236.
[9] H.-S. Ra, K.M. Ok, P.S. Halasyamani, J. Am. Chem. Soc. 125 (2003) 7764–7765.
[10] W. Zhang, X. Tao, C. Zhang, Z. Gao, Y. Zhang, W. Yu, X. Cheng, X. Liu, M. Jiang, Crystal Growth Des. 8 (2008) 307.
[11] Z. Gao, X. Tao, X. Yin, W. Zhang, M. Jiang, Appl. Phys. Lett. 93 (2008) 252906.
[12] Z. Gao, X. Yin, W. Zhang, S. Wang, M. Jiang, X. Tao, Appl. Phys. Lett. 95 (2009) 151107.
[13] X. Gonze, J.P. Vigneron, Phys. Rev. B 39 (1989) 13120.
[14] X. Gonze, Phys. Rev. A 52 (1995) 1086;
X. Gonze, Phys. Rev. A 52 (1995) 1096.
[15] The ABINIT code is a common project of the University Catholique de Louvain, Corning Incorporated, and other contributions (http://www.abinit.org).
[16] X. Gonze, Phys. Rev. B 55 (1997) 10337.
[17] X. Gonze, C. Lee, Phys. Rev. B 55 (1997) 10355.
[18] D. Vanderbilt, Phys. Rev. B 41 (1990) 7892.
[19] H.J. Monkhorst, J.D. Pack, Phys. Rev. B 13 (1976) 5188.
[20] J.P. Perdew, K. Burke, M. Ernzerhof, Phys. Rev. Lett. 77 (1996) 3865.
[21] N. Troullier, J.L. Martins, Phys. Rev. B 43 (1991) 1993.

[22] S. Baroni, P. Giannozzi, A. Testa, Phys. Rev. Lett. 58 (1987) 1861.
[23] S. Baroni, S. de Gironcoli, A.D. Corso, Rev. Mod. Phys. 73 (2001) 515.
[24] M. Veithen, X. Gonze, Ph. Ghosez, Phys. Rev. B 71 (2005) 125107.
[25] R. Resta, Rev. Mod. Phys. 66 (1994) 899.
[26] K.M. Rabe, C.H. Ahn, J.-M. Triscone (Eds.), Physics of Ferroelectrics: A Modern Perspective, Springer-Verlag, Berlin, Heidelberg, 2007.
[27] R. Resta, Europhys. News 28 (1997) 18.
[28] R.D. King-Smith, D. Vanderbilt, Phys. Rev. B 47 (1993) 1651.
[29] D. Vanderbilt, R.D. King-Smith, Phys. Rev. B 48 (1993) 4442.
[30] B. Xu, X. Li, J. Sun, L. Yi, J. Alloys Compd. 438 (2007) 25.
[31] B. Xu, X. Li, J. Sun, L. Yi, Eur. Phys. J. B 4 (2008) 483.
[32] Z.H. Levine, D.C. Allan, Phys. Rev. Lett. 63 (1989) 1719.
[33] R.O. Jones, O. Gunnarsson, Rev. Mod. Phys. 61 (1989) 689.
[34] M.Q. Cai, Z. Yin, M.S. Zhang, Appl. Phys. Lett. 83 (2003) 2805.